ACS OMEGA

Open Access

http://pubs.acs.org/journal/acsodf

Article

Modeling of Supercritical CO_2 Adsorption for Low-Permeability Coal Seam of Huainan−Huaibei Coalfield, China

Zhengpu Fan, Huihu Liu,* Junlin Liu, Sheng Xue,* Kun Zhang, Hongjie Xu, and Huihuang Fang

Cite This: *ACS Omega* 2023, 8, 44195−44211

Read Online

ACCESS | Metrics & More | Article Recommendations

ABSTRACT: Investigating the coal adsorption behavior on supercritical CO_2 ($ScCO_2$) is crucial for long-term CO_2 geological storage. In this paper, low-permeability coal samples from the Huainan−Huaibei coalfields in China were selected. The high-pressure isothermal adsorption of CO_2 was carried out at 36, 42, and 48 °C. The results of adsorption experiments were analyzed by fitting 9 types of modified adsorption models, including three different adsorption theories. Considering that different adsorption mechanisms may exist for CO_2 in coal, 14 mixed adsorption models were established. The accuracy of the coefficient of determination (R^2) and root-mean-square error (RMSE) for $ScCO_2$ excess adsorption capacity was analyzed, mainly focusing on the accuracy of the key model parameters such as the adsorption phase density and the theoretical adsorption capacity. These parameters were discussed, combined with the predicted adsorption phase density of CO_2 based on the intercept method. The results indicate that among the 9 types of modified adsorption considered, based on the adsorption phase density screening, the deviation of the predicted adsorption capacity from the experimental value was then considered. The Dubinin−Radushkevich (DR) model can effectively fit the adsorption behavior of CO_2 at low pressure (<7.5 MPa). The Langmuir (L), Langmuir−Freundlich (LF), Extended-Langmuir (EL), and TOTH models can effectively fit the adsorption behavior of CO_2 at high pressure (7.5−20 MPa), while the multimolecular layer models were unsuitable for fitting $ScCO_2$ adsorption. The model fitting results showed that only the monomolecular layer and micropore-filled adsorption models were suitable for fitting the $ScCO_2$ adsorption capacity. The DR-LF model best fits the adsorption data based on its key parameters of adsorption phase density and theoretical adsorption capacity. The established mixed model DR-LF fitting results showed that the CO_2 in coal was dominated by microporous filling adsorption. The higher the temperature, the greater the contribution of microporous filling adsorption to the total adsorption. There still exists deviation in the adsorption phase density and theoretical adsorption capacity. The contribution percentage of different adsorption mechanisms of CO_2 in coal needs to be further investigated.

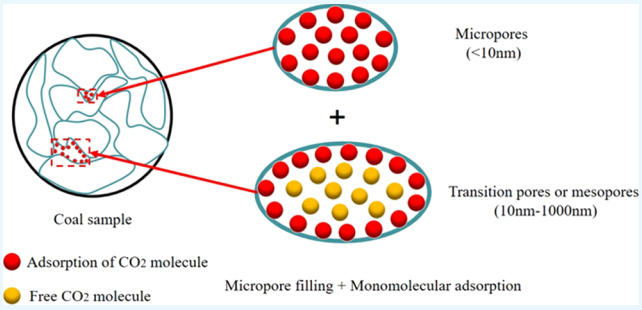

1. INTRODUCTION

To control the rise in CO_2 emissions, geological storage of CO_2 has become a significant focus both in China and internationally. CO_2 sequestration in coal seams has emerged as a reliable technical means for reducing the level of CO_2 emissions. As CO_2 has a higher adsorption capacity than CH_4, it can replace adsorption methane, and CO_2-ECBM technology can increase coalbed methane recovery rates while sequestering CO_2 to reduce greenhouse gas emissions.[1−3] However, with the CO_2-ECBM project advancing to deeper coalbed methane extraction, increasing temperature, and ground stress pressure, CO_2 can easily become the supercritical state (P > 7.38 MPa, T > 31.04 °C).[4] Many scholars and engineers use the adsorption model to fit the adsorption isotherm to find out the adsorption parameter and the Langmuir volume as the saturated adsorption capacity of coal to further carry out the theoretical and engineering practice research on the comparison of the accuracy of the coalbed gas adsorption model and the calculation of coalbed methane resources.

Indoor isothermal adsorption experiments are essential tools for assessing the adsorption gas content in coal. The curve of CO_2 adsorption capacity in coal versus pressure at a specific temperature can be obtained by simulating geological temperature and pressure conditions in this experiment. Two different adsorption isotherms have been obtained from many experimental tests: a Langmuir-type isotherm that rises to saturation capacity at low pressure and then forms a gentle straight line and

Received: September 4, 2023
Revised: October 8, 2023
Accepted: October 25, 2023
Published: November 10, 2023

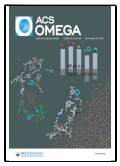

https://doi.org/10.1021/acsomega.3c06599
ACS Omega 2023, 8, 44195−44211

a decreasing isotherm that reaches peak adsorption capacity at high pressure. In these experiments, theories such as negative adsorption,[5] desorption-lagged adsorption,[6] and supercritical adsorption[7] have been proposed. The decrease in the "peak" adsorption isotherm is the subtraction of a portion of the Gibbs discarded from the mass of the adsorption phase, which is absolute adsorption.[8] The modified supercritical model requires multiplication by excess adsorption conversion expression $(1 - \rho_g/\rho_a)$. Therefore, the isothermal adsorption mathematical model is proposed to fit the experimental adsorption isotherm. The fitting parameters of the adsorption phase density and theoretical adsorption capacity with physical significance are obtained. The adsorption characteristics of coal are analyzed to evaluate the CO_2 adsorption capacity of the coal seam.

Many scholars in China and abroad have studied the characterization of mathematical models of gas adsorption in coal.[9−13] The Langmuir monomolecular adsorption model is widely used in various solid gas adsorption experiments. Bae et al.[14] studied the adsorption of CH_4 and CO_2 in coal at 40 °C and up to 20 MPa; they found that the Langmuir model was not as empirically extended as the Langmuir−Freundlich model, while the fitting deviation between the TOTH model and the adsorption data was smaller and the accuracy was higher. Some studies concluded that the conventional Langmuir model, which assumes a homogeneous adsorption surface and equal energy adsorption sites, is unable to explain the adsorption characteristics of CO_2 in coal under different pore sizes and different physicochemical environments. Tang et al.[15] studied the adsorption of CH_4 on shale up to 27 MPa at 82 °C, assumed the existence of two significantly different adsorption sites, and developed a dual adsorption site Langmuir-type adsorption model. Brunauer−Emmett−Teller (BET) multilayer adsorption theory is the same as the Langmuir monolayer adsorption theory, which still assumes that the solid surface is uniform. Wu et al.[16] studied the CO_2 adsorption of coal up to 13 MPa at 55 °C and found that the BET multimolecular layer model had a good fitting effect only at high-pressure 8−13 MPa. Some scholars[17,18] concluded that the BET multimolecular layer adsorption model could not describe micropores-dominated coal gas adsorption isotherms after fitting experimental data to these isotherms. Given the extreme development of micropores in coal, some scholars[19,20] consider that CO_2 was adsorbed in coal as micropore filling. Some scholars[21,22] consider that the D−A and D−R models based on micropore filling theory only consider the adsorption capacity adsorption inside the micropores but not the adsorption capacity of the macropore inside the coal.

The adsorption of CO_2 in coal may exist in several adsorption theories simultaneously due to their pore structure diversity.[23−26] The models described above are based on the assumption of a single adsorption theory, which cannot reflect the adsorption differences between different pore structures. Notably, Zhou et al.[23] conducted experiments on supercritical CH_4 adsorption from shale rocks and determined that the DR−Langmuir mixed model provided a better fit for supercritical CH_4 adsorption when compared to the micropores filling model and monomolecular layer model.

Presently, the majority of research on mixed adsorption models focuses on gas-derived rocks, primarily targeting shale gas. However, there is a significant gap in the literature regarding the application of mixed models to study the adsorption of $ScCO_2$ on coal. Moreover, the existing models for $ScCO_2$ adsorption on coal predominantly emphasize fitting accuracy while neglecting the error of various model parameters, adsorption phase density, and theoretical adsorption capacity. To address these research gaps, our study selected two low-permeability coal samples and conducted isothermal adsorption experiments using CO_2 at temperatures of 36, 42, and 48 °C, employing the weight method. The resulting experimental data were meticulously compared and fitted with different modified adsorption models, enabling us to evaluate the accuracy of the parameters of each model's parameters. To further unravel the CO_2 adsorption mechanism in coal under high-pressure conditions, we developed and compared various mixed adsorption models to effectively capture the $ScCO_2$ adsorption behavior. The optimal adsorption model was determined through comprehensive analysis and comparison of each model's parameters. This selection process provided a fundamental understanding of the pore structure control mechanism underlying $ScCO_2$ adsorption onto coal. The insights gained from this study enhance our understanding of the intricate mechanisms governing $ScCO_2$ adsorption in coal.

2. METHOD OF MODELING ON CO_2 ADSORPTION

2.1. Theoretical Basics of Modeling. The adsorption of gases on solid surfaces exhibits various states. In 1945, Brunauer classified adsorption isotherms into five types, commonly called the BDDT classification. Later, IUPAC[27] introduced a sixth type, the stepped isotherm, as shown in Figure 1. Most practical adsorption models are a combination of these six isotherm types. The 3 types of sorption theory models used in this paper are shown in Table 1.

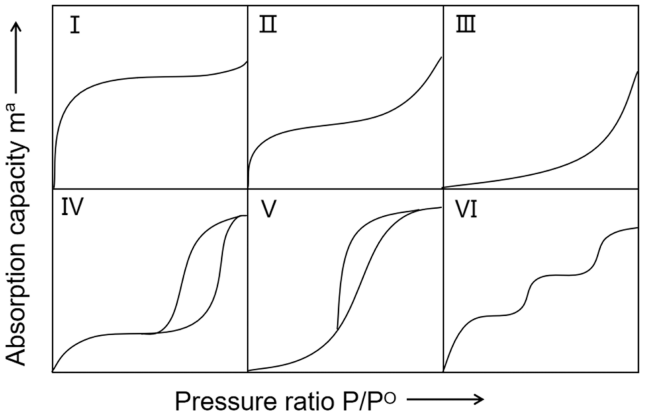

Figure 1. Six classifications of adsorption isotherms I−VI.

Langmuir established the monolayer adsorption model in 1916 when studying the basic characteristics of the adsorption of liquids and gases on solid surfaces.[28,29] The Langmuir model belongs to the type I isotherm in Figure 1, which means that at low adsorption pressures, the adsorption rate is fast due to the large surface area inside the micropores, and the isotherm gradually approaches equilibrium as the micropores become filled. Finally, the isotherm rise occurs due to the presence of gaps in the adsorption particles that are similar to the adsorption of large pores. The Langmuir model assumes that the adsorbent surface is uniform, the adsorption is monolayer, each adsorption site can only adsorb one molecule, and the adsorption sites can be uniformly distributed over the entire surface. To characterize the effects of different coal types, constants k and n related to the adsorbent, adsorbate, and temperature are introduced. Re-

https://doi.org/10.1021/acsomega.3c06599
ACS Omega 2023, 8, 44195−44211

Table 1. 9 Type Adsorption Models and Parameters[a]

model name	model equations	simulation parameters
L	$V = V_L \frac{P}{P_L + P}$	V_L, P_L
TOTH	$V = V_L \frac{k_b P}{[1 + (k_b P)^n]^{1/n}}$	V_L, K_b, n
LF	$V = V_L \frac{k_b P^n}{1 + k_b P^n}$	V_L, K_b, n
EL	$V = V_L \frac{k_b P}{1 + k_b P + n\sqrt{k_b P}}$	V_L, K_b, n
DL	$V = V_L\left[(1-\alpha)\frac{K_1 P}{1 + K_1 P} + \alpha \frac{K_2 P}{1 + K_2 P}\right]$	V_L, α, K_1, K_2
DBET	$V = V_m \frac{CP}{(P^0 - P)\left[1 + (C-1)\left(\frac{P}{P^0}\right)\right]}$	V_m, C
TBET	$V = V_m \frac{CP\left[1 - (n+1)\left(\frac{P}{P^0}\right)^n + n\left(\frac{P}{P^0}\right)^{n+1}\right]}{(P^0 - P)\left[1 + (C-1)\left(\frac{P}{P^0}\right) - C\left(\frac{P}{P^0}\right)^{n+1}\right]}$	V_m, C, n
DA	$V = V_0 \exp\left[-D \ln^n\left(\frac{P^0}{P}\right)\right]$	V_0, D, n
DR	$V = V_0 \exp\left[-D \ln^2\left(\frac{P^0}{P}\right)\right]$	V_0, D, n

[a]Note: V is the excess adsorption capacity at pressure balance, cm^3/g; P is the adsorption equilibrium pressure, MPa; P_L is the Langmuir pressure, MPa; V_0 is the microporous filling theoretical adsorption capacity, cm^3/g; D is the constant related; V_L is the Langmuir volume, cm^3/g; K_L is the Langmuir coefficient; K_b is the binding constant, $m^3 \cdot [t \cdot (MPa)^n]^{-1}$; k_1 and k_2 are the two types of adsorption sites; α is the percentage of each type of adsorption site; and n is the model parameter related to temperature and coal pore distribution. P^0 is the saturation vapor pressure, $P^0 = P_C(T/T_C)$, P_C = 7.38 MPa is the CO_2 critical pressure, and T_c = 304.25 K. V_m is the multimolecular layer theoretical adsorption capacity, cm^3/g; C is the constant related to the heat of adsorption and liquefaction of the adsorbate.

searchers have derived TOTH, Langmuir−Freundlich, and Extended-Langmuir adsorption models.[30,31]

Brunauer−Emmett−Teller extended the Langmuir monomolecular layer adsorption theory to the inverse S-shaped type II isotherm of the BET multimolecular layer adsorption. The implication is that, at low pressure, the macropores indicate that saturated monolayer adsorption occurs, followed by multimolecular layer adsorption starting as the pressure increases.[32] Finally, when saturation vapor pressure is nearing saturation, the number of adsorption layers increases rapidly, and the isotherm rises. BET multimolecular layer adsorption theory still assumes that the solid surface is uniform but believes that there are not only van der Waals forces between the adsorbent and the adsorbate but also van der Waals forces in the adsorbate, so multimolecular layer adsorption occurs.

The micropore filling theory model is based on the adsorption potential theory, which holds that the strong enhanced van der Waals forces caused by the overlapping of adsorbate surface adsorption potentials in micropores compress the adsorbate molecules into a high-density state within the micropore range, thus increasing the potential field of the opposing surfaces of numerous micropores in the carbonaceous adsorbent and strengthening the adsorption energy within the micropores of the carbonaceous adsorbent. This model is in accordance with the type I isotherm. Dubinin and Astakhov[33] proposed the DA micropore filling adsorption model, and Dubinin and Radushkevich[34] simplified the D−A model to the D−R model.

In isothermal adsorption studies below the critical temperature, the aforementioned isothermal adsorption models proposed by scholars based on different assumptions of adsorption mechanisms have been successfully applied. Still, the related models and theories face challenges when used for $ScCO_2$ isothermal adsorption in coal. The subcritical isothermal adsorption model is suitable for fitting monotonically increasing adsorption curves and cannot describe the decreasing adsorption curves under supercritical conditions. The modified supercritical model requires multiplication by the excess adsorption conversion expression $(1 - \rho_g/\rho_a)$[35]

$$V = (\text{adsorption model})(1 - \rho_g/\rho_a) \quad (1)$$

where ρ_g is the free phase density and ρ_a is the adsorption phase density.

Therefore, the modified supercritical adsorption model used in this paper should be extended to the supercritical isothermal adsorption category by multiplying the model in Table 1 by $(1 - \rho_g/\rho_a)$, which is used to fit the excess adsorption capacity.

2.2. Prediction Method of Adsorption Parameters Based on Gibbs Measurement of CO_2. Gibbs studied gas−solid surface adsorption. He proposed the theory of the adsorption phase and simplified the gas−solid adsorption experimental system into three parts: adsorbent, adsorption phase, and free phase. The adsorption phase in the system can expand a certain distance along the adsorbent surface and occupy a certain volume v_a because of the adsorption force. The density ρ_a of the adsorbent phase is not uniform, but the closer the distance from the adsorbent surface, the higher the adsorption phase density, and the farther the distance from the adsorbent surface, the more inclined to balance with the free phase density ρ_g. However, the interface of the adsorption phase and free phase cannot be distinguished in the present experiment,[36] so the mass of the adsorption phase m_a cannot be accurately measured. To solve this problem, Gibbs divided the mass of the adsorption phase into two parts,[37] as follows:

$$m_a = m_e + \rho_g v_a \quad (2)$$

From $m_a = \rho_a v_a$, we get

$$m_e = m_a(1 - \rho_g/\rho_a) \quad (3)$$

where m_e is the Gibbs excess adsorption capacity; $\rho_g v_a$ is the mass of matter with free phase density ρ_g occupying the adsorption phase volume v_a, defined as the Gibbs abandonment volume,[38] and its physical meaning is the portion of the actual adsorption capacity discarded from the adsorption phase.

The existing supercritical adsorption models are based on different adsorption equations, free phase densities, and adsorption phase densities combined with eq 3 to obtain various supercritical adsorption models describing Gibbs' adsorption.

Therefore, it is crucial to obtain the adsorption phase density accurately. The adsorption phase density is calculated using the following three methods: (i) the intercept method for the measured excess adsorption versus gas density curve, taking the intersection of the high-pressure falling section with the horizontal axis as the adsorption phase density; (ii) the adsorption phase density is empirically determined, e.g., atmospheric pressure boiling point liquid CO_2 density 1.18 g/cm^3 or obtained from an empirical formula; and (iii) the adsorption phase density is used as one of the fitting parameters

https://doi.org/10.1021/acsomega.3c06599
ACS Omega 2023, 8, 44195−44211

Figure 2. Geographical location of the test coal sample.

Table 2. Basic Physical Properties of Coal Samples

		maceral composition (wt %)			proximate (wt %)				
sample ID	$R_{o,max}$ (%)	vitrinite	inertinite	chitinite	M_{ad}	A_{ad}	V_{daf}	FC_d	coal type
LZ	0.93	84.84	11.74	3.42	1.25	19.60	39.34	39.81	gas coal
QD	0.93	79.68	15.35	4.97	0.88	11.02	38.59	49.51	fat coal

Table 3. Distribution of Pore Volume and Specific Surface Area in Coal Samples

		volume fraction (%)					percentage of surface area (%)			
sample ID	pore volume (cm^3/g)	micropore	transition pore	meso pore	macropore	surface area (m^2/g)	micropore	transition pore	meso pore	macropore
LZ	0.02	26.66	29.40	7.88	36.05	3.49	73.19	26.02	0.68	0.105
QD	0.027	32.30	20.46	7.75	39.48	4.93	71.99	27.31	0.61	0.083

obtained by fitting the excess adsorption to the adsorption model.

The intercept method takes advantage of the fact that the adsorption phase density tends to be constant in the linearly decreasing section of the Gibbs adsorption isotherm to solve for the adsorption phase density. Second, the liquid phase density method only considers the effect of temperature and pressure changes on adsorption. It is inaccurate to analogize the boiling point liquid phase density value of 1.18 g/cm^3 to the adsorption phase density. The adsorption model fitting method requires setting initial values and parameter ranges due to the large number of parameters, which may produce a human error. In summary, the intercept method is the only reliable way to back-calculate the adsorption phase density and theoretical adsorption capacity, relying solely on experimental data. The study carried out in this paper is an error analysis combining the adsorption phase density and the theoretical adsorption capacity obtained by the intercept method, including the analysis of the effect of fitting the CO_2 adsorption capacity using different adsorption models.

2.3. Experiments and Method. *2.3.1. Samples.* Two middle-grade metamorphic coal samples from the Liuzhuang coal mine and Qidong coal mine located in the Huainan−Huaibei coalfield areas are selected, as shown in Figure 2. The collected coal samples were crushed by crusher, sieved to 180−250 μm (60−80 mesh), dried in a dryer at 105 °C for 20 h, numbered as LZ and QD in the order of LiuZhuang and Qidong, and stored in coal sample bottles. The results of the industrial analysis of the coal samples are shown in Table 2. Low-temperature liquid nitrogen adsorption experiments were used to study the pore size distribution and specific surface areas of the coal samples. Since the decimal pore size classification criteria proposed by Hodot et al. is more suitable for characterizing the pore size distribution in coal,[39,40] this work adopted Hodot's pore classification scheme; the pore size distribution is divided into 4 types: micropores (<10 nm), transition pores (10−100 nm), mesopores (100−1000 nm), and macropores (>1000 nm). Table 3 shows the percentage of pore volume for the different types of pores and the percentage of surface area for the different types of pores. It can be seen that the main distribution interval is 0−100 nm. It is generally believed that CO_2 is adsorbed as a filling in the micropores and as a monolayer or multilayer in the meso- and macropores. The sum of the specific surface areas of the micropores and

https://doi.org/10.1021/acsomega.3c06599
ACS Omega 2023, 8, 44195−44211

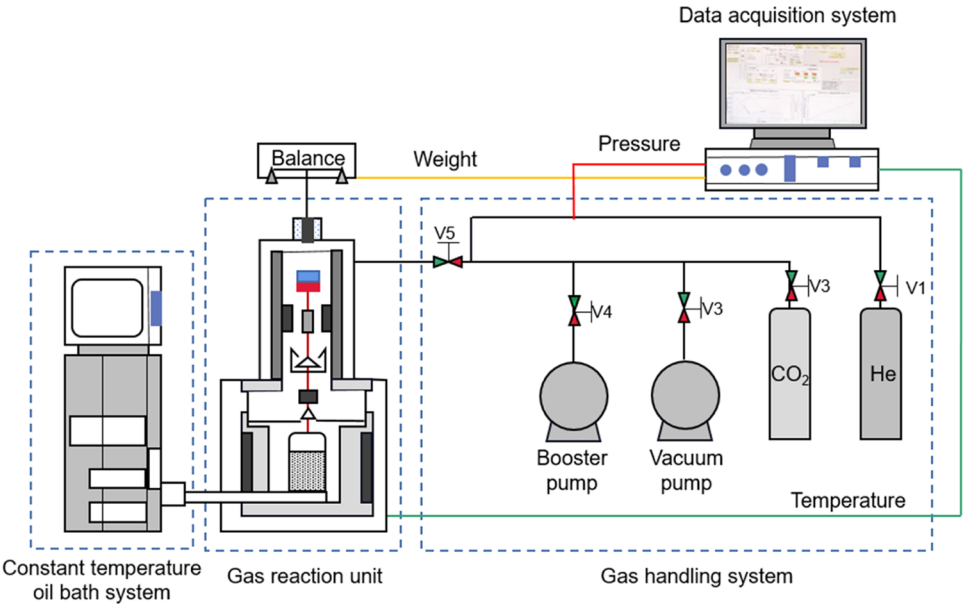

Figure 3. Principle of high-pressure isothermal adsorption experiments by the weight method.

mesopores of the two coal samples accounted for more than 99% of the total specific surface area. Since the specific surface area mainly influences the adsorption capacity, it can be assumed that the adsorption gas is mainly stored in the micropores and mesopores.

2.3.2. Experimental Principles. The isothermal adsorption test of coal was conducted using a high-pressure isothermal adsorption apparatus with the weight method. The weight method was employed to measure the mass of the adsorption sample directly. The schematic diagram of the experimental setup is presented in Figure 3. The maximum test pressure was set at 40 MPa, the maximum test temperature at 150 °C, and the magnetic levitation balance reading accuracy was 0.01 mg, which fulfills the requirements of this study. The adsorption capacity was calculated by measuring the change in sample mass before and after adsorption, based on Archimedes' principle, using a high-precision magnetic levitation balance.

Based on the requirement that the temperature and pressure conditions for storing $scCO_2$ can only be achieved at depths of over a kilometer in coal seams, the experimental temperatures were set at 36, 42, and 48 °C, corresponding to the on-site temperature and pressure conditions. The experimental pressure range was set from 0 to 20 MPa, with pressure points ranging from subcritical to supercritical states of CO_2, including 0.5, 1.0, 2.0, 3.0, 4.0, 5.0, 6.0, 7.5, 9.0, 10.5, 12.0, 13.5, 15.0, 17.5, and 20.0 MPa. Each pressure point was set to ensure a sufficient adsorption equilibrium time for measuring the adsorption-saturated sample mass change. The high-pressure isothermal adsorption test with this apparatus involved four main steps: blank test, pretreatment, buoyancy test, and adsorption test. The amount of CO_2 adsorption on the coal sample was determined using the following equation.

$$m_a = \Delta m - m_s - m_b + \rho_g(v_s + v_b + v_a) \tag{4}$$

where m_a is the adsorption CO_2 mass, g; Δm is the magnetic levitation balance reading, g; m_s is the sample mass, g; m_b is the sample bucket mass, g; ρ_g is the free gas phase density at different pressure points, g/cm^3; v_s is the sample volume, cm^3; v_b is the sample bucket volume, cm^3; v_a is the adsorption phase volume, cm^3.

The blank test gives the sample bucket mass and volume, and as the blank test has no coal sample or adsorption phase, eq 4 can be simplified to eq 5. A linear fit was made to the Δm and ρ_g data read from the maglev balance to obtain its intercept as the sample bucket mass and slope as the sample bucket volume, providing the base data for the CO_2 high-pressure isothermal adsorption test.

$$\Delta m = m_s - p_g v_s \tag{5}$$

The buoyancy test provides measurements for the sample mass and volume during the experiment, where a coal sample is loaded. Since there is no adsorption of helium, eq 4 can be simplified to eq 6. A linear regression of the Δm and ρ_g data, obtained from the magnetic levitation balance, yields an intercept of $m_s + m_b$ and a slope of $v_s + v_b$. Combining the mass and volume of the sample bucket obtained from the blank test can determine the sample mass and sample volume.

$$\Delta m = (m_s + m_b) - \rho_g(v_s + v_b) \tag{6}$$

In the adsorption experiment, the volume of the adsorption phase V_a in eq 3 cannot be obtained experimentally, so the absolute adsorption capacity m_a cannot be obtained experimentally. According to the Gibbs excess adsorption volume m_e, the practical meaning of which is the amount of free phase gas density removed from the adsorption phase gas, the relationship between the excess adsorption capacity m_e and the absolute adsorption capacity m_a can be obtained from eq 2 as follows:

$$m_e = m_a - \rho_g v_a \tag{7}$$

Equation 7 can be simplified to the following equation to obtain the isothermal adsorption test results for the excess adsorption of CO_2 by coal

$$m_e = \Delta m - m_s - m_b + \rho_g(v_s + v_b) \tag{8}$$

Due to the presence of many pore structures in the coal, the adsorption of CO_2 into the coal will cause the matrix to undergo different degrees of expansion and deformation, resulting in a

https://doi.org/10.1021/acsomega.3c06599
ACS Omega 2023, 8, 44195−44211

Table 4. Mixed Adsorption Models with Three Types of Adsorption Theories

model name	model equations
DA-L	$V = \left[\lambda V_S \exp\left[-D\ln^{n1}\left(\frac{P^0}{P}\right)\right] + (1-\lambda)V_S\frac{P}{P_L+P}\right]\left(1-\frac{\rho_g}{\rho_a}\right)$
DA-TOTH	$V = \left[\lambda V_S \exp\left[-D\ln^{n1}\left(\frac{P^0}{P}\right)\right] + (1-\lambda)V_S\frac{K_bP}{[1+(K_bP)^n]^{1/n}}\right]\left(1-\frac{\rho_g}{\rho_a}\right)$
DA-LF	$V = \left[\lambda V_S \exp\left[-D\ln^{n1}\left(\frac{P^0}{P}\right)\right] + (1-\lambda)V_S\frac{K_bP^n}{1+K_bP^n}\right]\left(1-\frac{\rho_g}{\rho_a}\right)$
DA-EL	$V = \left[\lambda V_S \exp\left[-D\ln^{n1}\left(\frac{P^0}{P}\right)\right] + (1-\lambda)V_S\frac{K_bP}{1+K_bP+n\sqrt{K_bP}}\right]\left(1-\frac{\rho_g}{\rho_a}\right)$
DA-DL	$V = \left[\lambda V_S \exp\left[-D\ln^{n1}\left(\frac{P^0}{P}\right)\right] + (1-\lambda)V_S\left[(1-\alpha)\frac{K_1P}{1+K_1P} + \alpha\frac{K_2P}{1+K_2P}\right]\right]\left(1-\frac{\rho_g}{\rho_a}\right)$
DA-L	$V = \left[\lambda V_S \exp\left[-D\ln^{2}\left(\frac{P^0}{P}\right)\right] + (1-\lambda)V_S\frac{P}{P_L+P}\right]\left(1-\frac{\rho_g}{\rho_a}\right)$
DR-TOTH	$V = \left[\lambda V_S \exp\left[-D\ln^{2}\left(\frac{P^0}{P}\right)\right] + (1-\lambda)V_S\frac{K_bP}{[1+(K_bP)^n]^{1/n}}\right]\left(1-\frac{\rho_g}{\rho_a}\right)$
DR-LF	$V = \left[\lambda V_S \exp\left[-D\ln^{2}\left(\frac{P^0}{P}\right)\right] + (1-\lambda)V_S\frac{K_bP^n}{1+K_bP^n}\right]\left(1-\frac{\rho_g}{\rho_a}\right)$
DR-EL	$V = \left[\lambda V_S \exp\left[-D\ln^{2}\left(\frac{P^0}{P}\right)\right] + (1-\lambda)V_S\frac{K_bP}{1+K_bP+n\sqrt{K_bP}}\right]\left(1-\frac{\rho_g}{\rho_a}\right)$
DR-DL	$V = \left[\lambda V_S \exp\left[-D\ln^{2}\left(\frac{P^0}{P}\right)\right] + (1-\lambda)V_S\left[(1-\alpha)\frac{K_1P}{1+K_1P} + \alpha\frac{K_2P}{1+K_2P}\right]\right]\left(1-\frac{\rho_g}{\rho_a}\right)$
DA-DBET	$V = \left[\lambda V_S \exp\left[-D\ln^{n1}\left(\frac{P^0}{P}\right)\right] + (1-\lambda)V_S\frac{CP}{(P^0-P)\left[1+(C-1)\left(\frac{P}{P^0}\right)\right]}\right]\left(1-\frac{\rho_g}{\rho_a}\right)$
DA-TBET	$V = \left[\lambda V_S \exp\left[-D\ln^{n1}\left(\frac{P^0}{P}\right)\right] + (1-\lambda)V_S\frac{CP\left[1-(n+1)\left(\frac{P}{P^0}\right)^n+n\left(\frac{P}{P^0}\right)^{n+1}\right]}{(P^0-P)\left[1+(C-1)\left(\frac{P}{P^0}\right)-C\left(\frac{P}{P^0}\right)^{n+1}\right]}\right]\left(1-\frac{\rho_g}{\rho_a}\right)$
DR-DBET	$V = \left[\lambda V_S \exp\left[-D\ln^{2}\left(\frac{P^0}{P}\right)\right] + (1-\lambda)V_S\frac{CP}{(P^0-P)\left[1+(C-1)\left(\frac{P}{P^0}\right)\right]}\right]\left(1-\frac{\rho_g}{\rho_a}\right)$
DR-TBET	$V = \left[\lambda V_S \exp\left[-D\ln^{2}\left(\frac{P^0}{P}\right)\right] + (1-\lambda)V_S\frac{CP\left[1-(n+1)\left(\frac{P}{P^0}\right)^n+n\left(\frac{P}{P^0}\right)^{n+1}\right]}{(P^0-P)\left[1+(C-1)\left(\frac{P}{P^0}\right)-C\left(\frac{P}{P^0}\right)^{n+1}\right]}\right]\left(1-\frac{\rho_g}{\rho_a}\right)$

smaller pore structure and affecting the measured values. However, this effect will decrease with increasing temperature and pressure.[41]

2.3.3. Experimental Procedure. The high-pressure isothermal adsorption experiment by weight consists of several key steps, outlined as follows:

(1) Blank test: a blank test was conducted without a sample, wherein only the sample drum was placed in a reaction cell with helium gas as the medium. The temperature was set at 36 °C, consistent with subsequent isothermal adsorption tests. Eight pressure points were established in the 0−7.5 MPa range to obtain balance readings at different pressures. The balance readings were linearly fitted to the helium density to determine the mass and volume of the sample drum. Blank experiments were not required for each test. Only the mass and volume of the unique material sample drums in the laboratory were obtained. The effects of temperature and pressure on the drums' mass and volume were neglected.

(2) Sample pretreatment: an appropriate capacity of the sample, approximately 3 g in mass, was filled into a sample drum and subjected to vacuum degassing at 110 °C for 5 h to eliminate gas and water vapor adsorption on the original sample.

(3) Buoyancy test: after pretreatment, helium gas was introduced, and eight pressure points were set in the range of 0−7.5 MPa to obtain balance readings at different pressures. The balance readings were linearly fitted to the helium density to determine the combined mass and volume of the sample bucket and sample. By combining this information with the mass and volume of the sample

https://doi.org/10.1021/acsomega.3c06599
ACS Omega 2023, 8, 44195−44211

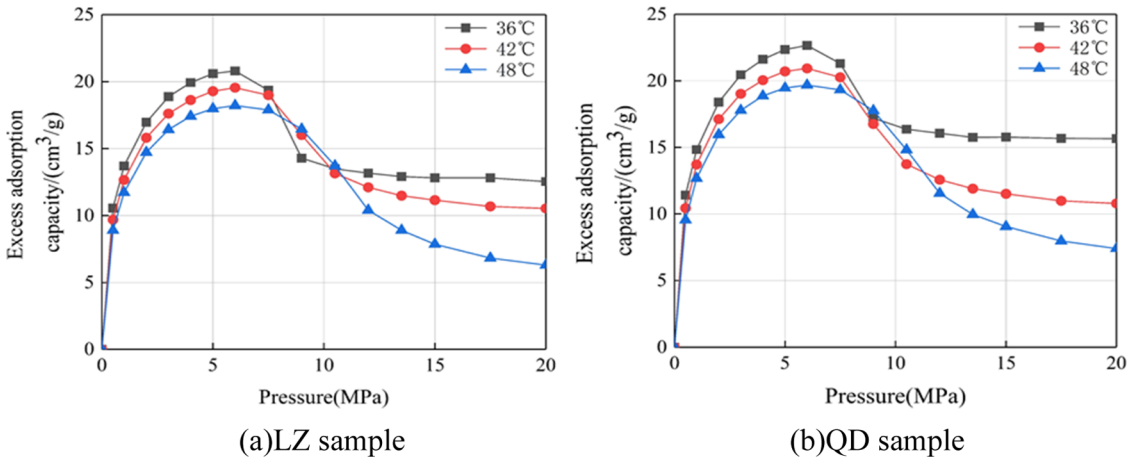

Figure 4. High-pressure isothermal adsorption curve of coal on CO_2 before calibration.

Table 5. Results of the Adsorption Phase Density and Theoretical Adsorption Capacity Fit

sample ID	experimental temperature (°C)	linear equations	coefficient of determination R^2	adsorption phase density (g/cm^3)	$V_a\rho_a$ (cm^3/g)
LZ	36	$y = -11.996x + 22.445$	0.9896	1.8710	22.445
	42	$y = -13.724x + 21.697$	0.9979	1.5810	21.697
	48	$y = -18.914x + 21.719$	0.9832	1.1483	21.719
QD	36	$y = -10.287x + 24.031$	0.9898	2.3361	24.031
	42	$y = -15.327x + 23.264$	0.9973	1.5178	23.264
	48	$y = -19.458x + 23.214$	0.9867	1.1930	23.214

drum obtained in the buoyancy test, the mass and volume of the experimental sample could be determined.

(4) Adsorption test: the adsorption test was carried out using 99.99% pure CO_2 at 15 pressure points ranging from 0 to 20 MPa. The measurements were conducted from vacuum to the target pressure following a preset pressure path. The equilibration time for each pressure point was 4 h to ensure pressure stability during CO_2 adsorption.

2.4. Modeling Procedure of the Mixed Adsorption Model. Although the existing adsorption models using established adsorption equations have shown high stability and accuracy, the Langmuir adsorption equation and its modified forms describe the adsorption mechanism as monolayer adsorption on the surface; the BET equation describes multilayer adsorption, and the D−R and D−A equations describe the mechanism as micropore filling. However, due to the diverse pore structure of coal, it is speculated that CO_2 adsorption in coal occurs through a combination of monolayer adsorption, multilayer adsorption, and micropore filling.[42]

Therefore, different adsorption theories and equations must be combined to characterize the CO_2 adsorption mechanism in coal. To investigate the representation of supercritical CO_2 adsorption using a mixed adsorption model, the adsorbate phase density function was combined with nine different adsorption equations, resulting in the development of new models that incorporate multiple adsorption mechanisms for the characterization of supercritical CO_2 adsorption in coal. The expression of the model is as follows:

$$V = [\lambda V_S(\text{adsorption model}) + (1 - \lambda) V_S(\text{adsorption model})](1 - \rho_g/\rho_a) \quad (9)$$

where λ $(0 < \lambda < 1)$ is the contribution proportion of different adsorption theoretical models to the adsorption capacity; V_S is the sum of the theoretical adsorption capacity of the two adsorption theories.

Two coal samples' high-pressure adsorption curves were also selected for comparative evaluation at temperatures of 36, 42, and 48 °C. The following three items were evaluated and compared: (i) the comparison of the coefficient of determination (R^2) of excess adsorption and the fitting error analysis of the adsorption capacity; (ii) the comparison analysis of adsorption data at three temperatures fitted by different adsorption models and the adsorption phase density by the intercept method; and (iii) the comparison analysis of the fitting effect of the mixed model and the best-mixed adsorption model was selected. Fourteen improved coal CO_2 high-pressure adsorption mixed models are given in Table 4.

3. RESULTS

The CO_2 adsorption capacity that can be measured in the experiment is the excess adsorption capacity. The curve of the excess adsorption capacity of coal obtained in the isothermal adsorption test is shown in Figure 4(a,b). The actual adsorption capacity is the absolute adsorption capacity. In this paper, the adsorption phase density obtained by the intercept method and various adsorption model methods will be used to correct the absolute adsorption capacity, respectively, and the applicability of various adsorption model correction methods in the gravimetric measurement of CO_2 adsorption by coal will be analyzed by comparing with intercept method. Based on the linear equation fitting between the CO_2 excess adsorption capacity and free phase density in the descending section of high-pressure adsorption, the CO_2 adsorption phase density ρ_a and theoretical adsorption capacity $V_a\rho_a$ obtained in this study are from the fitting linear equation, shown in Table 5. The fitting results show that when the temperature increases from 36 to 48

https://doi.org/10.1021/acsomega.3c06599
ACS Omega 2023, 8, 44195−44211

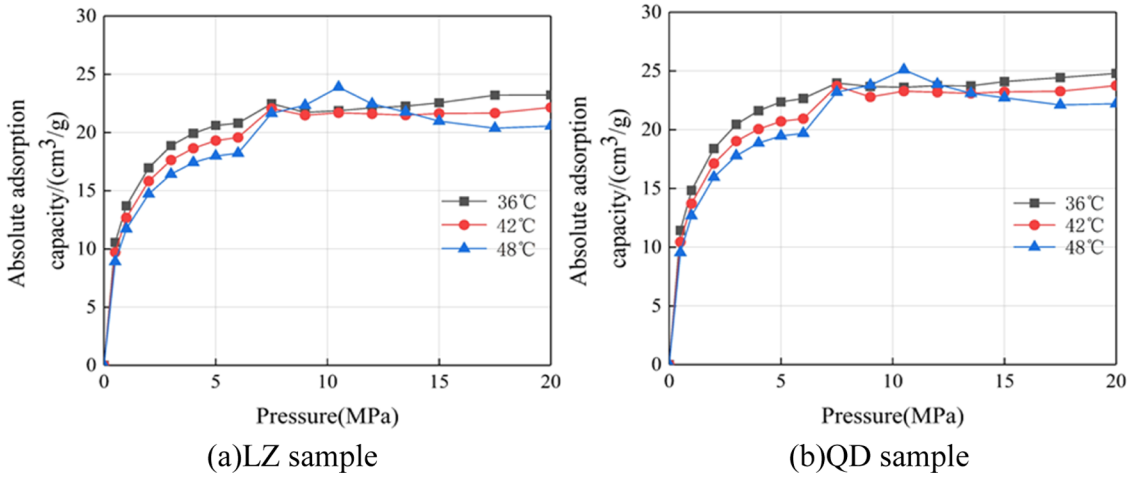

Figure 5. Calibrated coal-to-CO_2 high-pressure isothermal adsorption curve.

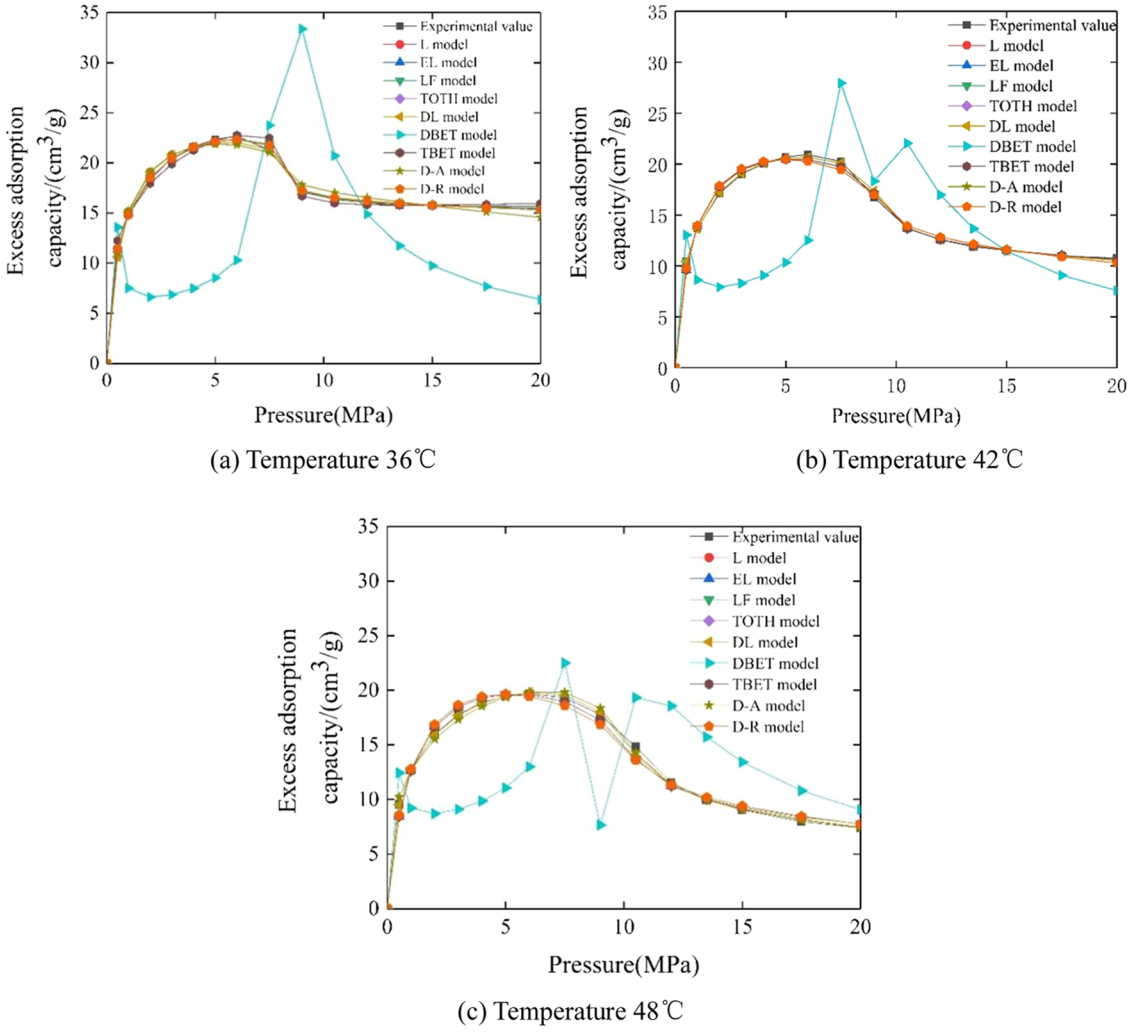

Figure 6. QD sample modified adsorption theory model fitted excess adsorption curve.

°C, the adsorption phase density of the LZ coal sample decreases from 1.8710 to 1.1483 g/cm^3, and that of the QD coal sample decreases from 2.3361 to 1.1930 g/cm^3. It can be seen that an increase in temperature will lead to a decrease in the adsorption phase density of CO_2. The adsorption phase density of the CO_2 is 1.1483 to 2.3361 g/cm^3, which is between the critical density of CO_2 and the boiling point liquid density at atmospheric pressure, indicating the CO_2 adsorption phase densities obtained by the intercept method are accurate.

From Figure 4(a,b), it can be seen that the CO_2 excess adsorption capacity inflects at CO_2 pressure 7−8 MPa, respectively, and the excess adsorption capacity appears to

https://doi.org/10.1021/acsomega.3c06599
ACS Omega 2023, 8, 44195−44211

Table 6. Single Adsorption Theory Model Coefficient of Determination (R^2) and Root-Mean-Square Error (RMSE)

temperature (°C)		L model	EL model	LF model	DL model	TOTH model	TBET model	DBET model	D−A model	D−R model
36	R^2	0.9954	0.9954	0.9954	0.9987	0.9954	0.078	0.9954	0.9926	0.9891
	RMSE	0.989	0.989	0.989	0.807	0.989	26.494	0.989	1.246	1.513
42	R^2	0.9954	0.9954	0.9954	0.9993	0.9954	0.1898	0.9954	0.9932	0.9932
	RMSE	0.992	0.992	0.992	0.768	0.992	18.156	0.992	1.203	1.204
48	R^2	0.9910	0.9910	0.9910	0.9984	0.9910	0.1481	0.9910	0.9959	0.9970
	RMSE	1.554	1.554	1.554	0.814	1.554	15.654	1.554	0.883	0.840

Table 7. Monomolecular Layer Adsorption Theory and Micropores Filling Theory Model Fitted Parametric Adsorption Phase Density Standard Error with Intercept Method

	36 °C		42 °C		48 °C		
adsorption model	LZ	QD	LZ	QD	LZ	QD	average
L	0.216	0.121	0.070	0.076	0.034	0.028	0.091
EL	0.216	0.121	0.070	0.076	0.034	0.028	0.091
LF	0.216	0.121	0.070	0.076	0.034	0.028	0.091
DL	0.394	0.251	0.135	0.165	0.124	0.125	0.199
TOTH	0.216	0.121	0.070	0.076	0.034	0.028	0.091
DA	0.788	0.487	0.155	0.346	0.174	0.153	0.350
DR	0.446	0.241	0.155	0.191	0.106	0.153	0.215

decrease. The relationship between excess adsorption capacity and absolute adsorption capacity is described in eq 2, which elucidates the decline of excess adsorption capacity with increasing adsorption phase density. In the subcritical state, the density of the CO_2 gas phase significantly differs from that of the adsorption phase, resulting in ρ_g/ρ_a approaching 0. As a result, the disparity between excess and absolute adsorption capacity is minimal, necessitating correction only in the high-pressure section. After correction, the absolute adsorption capacity curve was obtained using the intercept method, as illustrated in Figure 5(a,b). Notably, the absolute adsorption capacity does not decrease with increasing pressure, indicating that the excess adsorption capacity must exhibit a maximum value, followed by a gradual decrease with the pressure increment.

4. DISCUSSION

4.1. Analysis of Modified Adsorption Model Fitting. This study utilized the professional nonlinear fitting software 1Stopt to optimally fit the experimental data of excess sorption using the Levenberg−Marquardt algorithm based on 9 modified adsorption models. To ensure the physical meaningfulness of the fitted parameters, V_L, V_0, V_m, P_L, K_L, K_b, n, P, C, K_1, and K_2 were constrained to positive values. Additionally, parameter n in the exponential functions of the TOTH, LF, TBET, and D−A models was set to nonzero positive integers. A comparison of the experimental and fitted results for the QD samples at temperatures of 36, 42, and 48 °C is presented in Figure 6(a−c). The coefficient of determination (R^2), root-mean-square error (RMSE), and CO_2 adsorption phase density, obtained through the 9 modified adsorption models fitting results, are shown in Table 6.

As illustrated in Figure 6 and the data in Table 6, the multimolecular layer adsorption theory DBET model poorly fits the $ScCO_2$ adsorption isotherm. In the parameters of the TBET model, $n = 1$, it is equivalent to the Langmuir model. Therefore, the multimolecular layer theoretical model is unsuitable for fitting the $ScCO_2$ adsorption isotherm. This finding of the theoretical adsorption model of multimolecular layers is consistent with previous research literature.[17] The modified models R^2 show that 5 types of monomolecular layer theoretical models and 2 types of microporous filling theoretical models are greater than 0.989, which has an excellent fitting effect. To further analyze the fitting effect of each model, the root-mean-square error (RMSE) was introduced, and it was found that the improved monomolecular layer theory EL, LF, DL, TOTH model RMSE was superior to the L model, and the improved micropores filling theory DA model RMSE was superior to the DR model. With the increase in temperature, it can be found that the fitting effect of the micropore filling model becomes better than that of the monomolecular layer model, which may be because the increase in temperature is more conducive to the adsorption of $ScCO_2$ by micropores. Based on the above analysis, the fitting of the L, EL, LF, DL, TOTH, D−A, and D−R models for $ScCO_2$ adsorption is effective.

Table 6 shows that the D−A model fits better than the D−R model for the micropores filling theory, and the EL, LF, DL, and TOTH models fit better than the Langmuir model for the monolayer adsorption theory. This is mainly because the D−A, EL, LF, DL, and TOTH models are improved models with more parameters and a higher degree of fit. However, the multi-parameter iterations require artificially set initial values and ranges for each parameter, which may lead to errors in the physical meaning of each parameter. The coefficient of determination (R^2) and root-mean-square error (RSEM) only describe the fitted model's accuracy and cannot determine the exact physical meaning of the fitted equation. Furthermore, in the correction of absolute adsorption, the adsorption phase CO_2 density directly affects the corrected absolute adsorption, and its reasonable value is significant. In this paper, the accuracy of each model is evaluated in terms of the standard error (S) of adsorption phase density fitted to the model. As there is no accurate definition of adsorption phase density, the only reliable intercept method is used to do error analysis on the adsorption phase density obtained from the experimental data in Table 5. The expression for the standard error (S) of adsorption phase density is as follows:

https://doi.org/10.1021/acsomega.3c06599
ACS Omega 2023, 8, 44195−44211

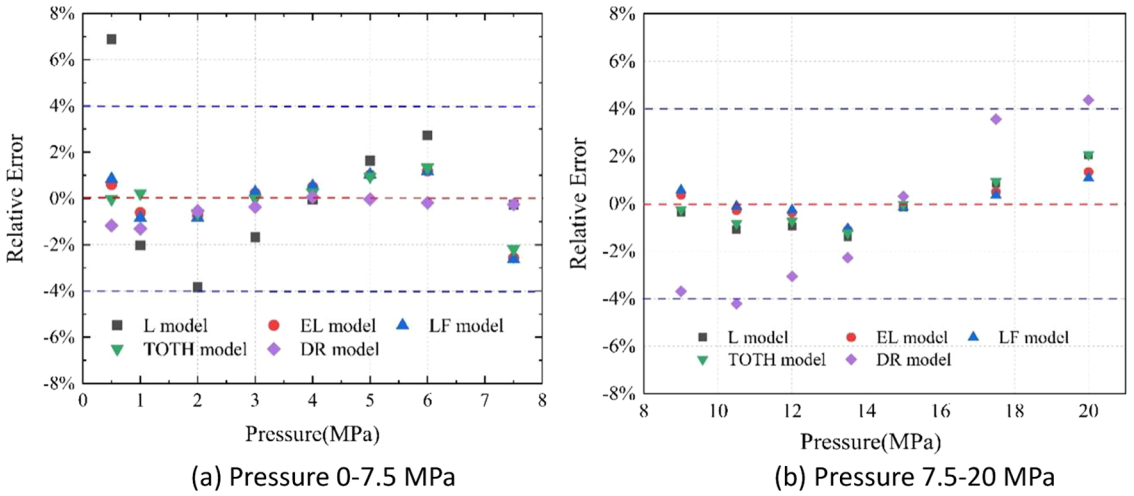

Figure 7. Relative error of segmentally fitted excess adsorption capacity of modified adsorption models.

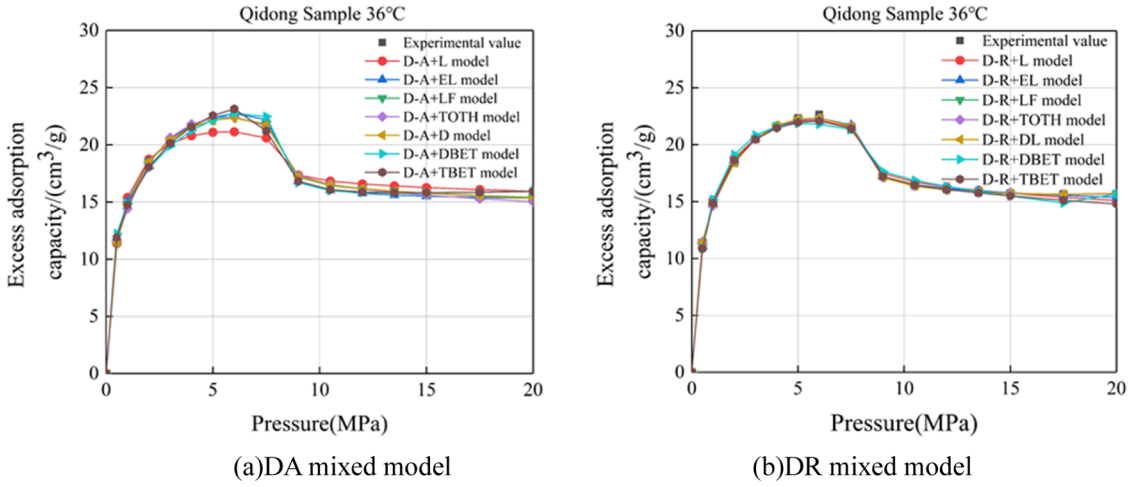

Figure 8. Fitted excess adsorption curves of mixed adsorption mechanism models.

$$S = \left[1/n \sum_{i=1}^{n} (\rho_i - \rho_e)^2\right]^{1/2} \quad (10)$$

where S is the standard error, n is the number of data points, and ρ_i and ρ_e are the intercept method and fitted value of the adsorption phase density at each temperature point, respectively.

To further analyze the accuracy of L, EL, LF, DL, TOTH, D−A, and D−R models, the fitted parametric adsorption phase density S values of LZ and QD coal samples at 36, 42, and 48 °C were calculated, as shown in Table 7, respectively, the smaller the S value, the higher the degree of accuracy. Among the five monomolecular layer theory models, the degree of accuracy of the parametric adsorption phase density was L = LF = EL = TOTH > DL. Among the two micropore filling theory models, the degree of accuracy of the parametric adsorption phase density was DR > DA. It can be seen that the adsorption phase densities fitted by the L, LF, EL, TOTH, and DR models fitted to the LZ and QD coal samples at the three temperatures have good stability, and their corrected absolute adsorption capacities would be more accurate. The deviations in their fitted adsorption phase densities may be because the adsorption mechanisms of $ScCO_2$ in coal with the porous structure are both micropores filling and monomolecular layer adsorption.

To verify the validity of the above assumptions, the L, LF, EL, and TOTH models of the monolayer theory and DR of the micropores filling theory, which was preferentially selected based on the deviation of the adsorption phase density of the model parameters as described above, were selected to segmentally fit the experimental results of the excess adsorption of QD samples at 36 °C. The relative errors between the fitted excess adsorption amounts and the experimental results were calculated for the subcritical pressure of 0−7.5 MPa and the supercritical pressure of 7.5−20 MPa for the preferred five modified models, respectively. As shown in Figure 7(a), the relative errors of the DR model of the micropore filling theory were all less than 2% at the subcritical pressure stage, and their average relative errors of 0.49% were also smaller than those of each of the monomolecular layer theoretical models. It shows that the micropore filling theory is more suitable for predicting coal adsorption on CO_2 in the low-pressure stage. It is stated in the literature[43] that the adsorption mechanism of $ScCO_2$ adsorption on coal tends to follow the monolayer adsorption theory, while the microporous filling theory is more applicable to subcritical CO_2. As shown in Figure 7(b), in the supercritical pressure stage, the relative errors of excess adsorption for the four monomolecular layer theory models were less than 2%. The average relative errors of excess adsorption for the L, LF, EL, and

https://doi.org/10.1021/acsomega.3c06599
ACS Omega 2023, 8, 44195−44211

Table 8. Comparison of the R^2, RMSE, and Micropore Filling Proportion (λ) of the Mixed Adsorption Model for Fitting Excess Adsorption Capacity

	R^2		RMSE		λ	
adsorption model	LZ	QD	LZ	QD	LZ	QD
DA-L	0.9986	0.9989	0.516	0.480	0.135	0.373
DA-EL	0.9978	0.9964	0.669	0.887	0.260	0.592
DA-LF	0.9983	0.9989	2.362	0.876	0.881	0.373
DA-TOTH	0.9989	0.9989	0.339	0.3669	0.677	0.664
DA-DL	0.9994	0.9994	0.338	0.340	0.085	0.053
DA-DBET	0.8824	0.8826	4.692	4.966	1	1
DA-TBET	0.8232	0.6685	5.776	8.657	1	1
DR-L	0.9953	0.9963	0.941	0.888	0.052	0.645
DR-EL	0.9953	0.9987	0.941	0.531	0.052	0.189
DR-LF	0.9962	0.9970	0.605	0.618	0.558	0.557
DR-TOTH	0.9953	0.9963	0.941	0.888	0.052	0.050
DR-DL	0.9942	0.9963	1.040	0.889	0.121	0.053
DR-DBET	0.9911	0.9925	26.420	1.254	1	1
DR-TBET	0.8668	0.9835	5.346	3.683	1	1

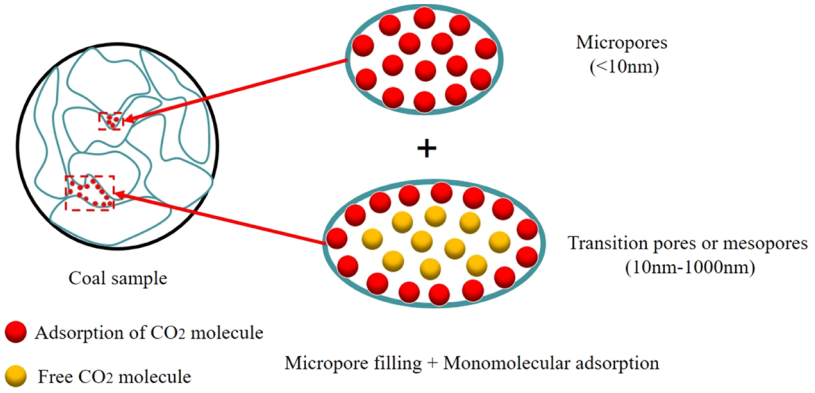

Figure 9. Schematic representation of the mixed adsorption mechanism of coal on $ScCO_2$.

TOTH models were 0.98, 0.58, 0.51, and 0.87%, respectively and were less than 3.07% for the DR model, indicating that the monolayer theory is more suitable for predicting coal-to-CO_2 adsorption under high-pressure conditions. Therefore, it is speculated that the micropore filling theory contributes more to coal for CO_2 adsorption at low pressure. In contrast, the monomolecular layer theory contributes more to coal for CO_2 adsorption at high pressures, and the mixture of the two adsorption theories may produce a better fit.

4.2. Analysis of Mixed Model Fitting. Whether the adsorption mechanism of $ScCO_2$ in nanopores is a mixed adsorption mechanism superposition model can be further investigated by fitting each mixed adsorption model. The excess adsorption data of the QD and LZ samples were fitted with the 14 mixed models in Table 4 at 36 °C. The fitted excess adsorption curve was compared with the experimental data, as shown in Figure 8(a,b). The 14 mixed adsorption models R^2, RMSE, and the proportion λ of theoretical adsorption by micropores filling are shown in Table 8.

As seen from Table 8, R^2 of QD and LZ samples is greater than 0.995 in the mixed model of micropore filling theory and monolayer theory at 36 °C, showing an excellent fitting effect. The RMSE of QD and LZ samples in the mixed model of microporous filling and multimolecular layer theory is much higher than that in the mixed model of microporous filling theory and single molecular layer theory, indicating that the mixed adsorption mechanism of microporous filling theory and single molecular layer theory is suitable for fitting the excess adsorption amount of $ScCO_2$ from coal.

Among the 14 types of mixed adsorption models, we further analyze the contribution of different adsorption mechanisms to $ScCO_2$ adsorption in coal. Table 8 shows the proportion of microporous filling adsorption in QD and LZ samples when the microporous filling proportion λ is 36 °C. λ is 1 in the DA-DBET and DR-TBET models, indicating that only micropore filling contributes to the adsorption of $ScCO_2$ in coal when using the micropore filling and the multimolecular layer theoretical adsorption model fit. Therefore, the adsorption mechanisms of the DA-DBET and DR-TBET models are unsuitable for characterizing $ScCO_2$ adsorption by coal.

In summary, the mechanism of $ScCO_2$ adsorption by coal is believed to involve both micropore filling and monomolecular adsorption, as illustrated in Figure 9. The adsorption process of CO_2 molecules in the nanopores of coal can be described as follows: at low pressures, CO_2 molecules are primarily adsorption on the high-energy adsorption sites (micropores) in the form of micropore filling, leading to a rapid increase in adsorption. As the pressure increases, the high-energy sites become occupied, and CO_2 molecules begin to adsorb onto the lower-energy adsorption sites (transition pores and mesopores). With a further pressure increase, both monomolecular adsorption and micropore filling occur simultaneously, as CO_2 molecules continue to adsorb onto the lower-energy adsorption sites. From an adsorption potential perspective, the curvature of

https://doi.org/10.1021/acsomega.3c06599
ACS Omega 2023, 8, 44195−44211

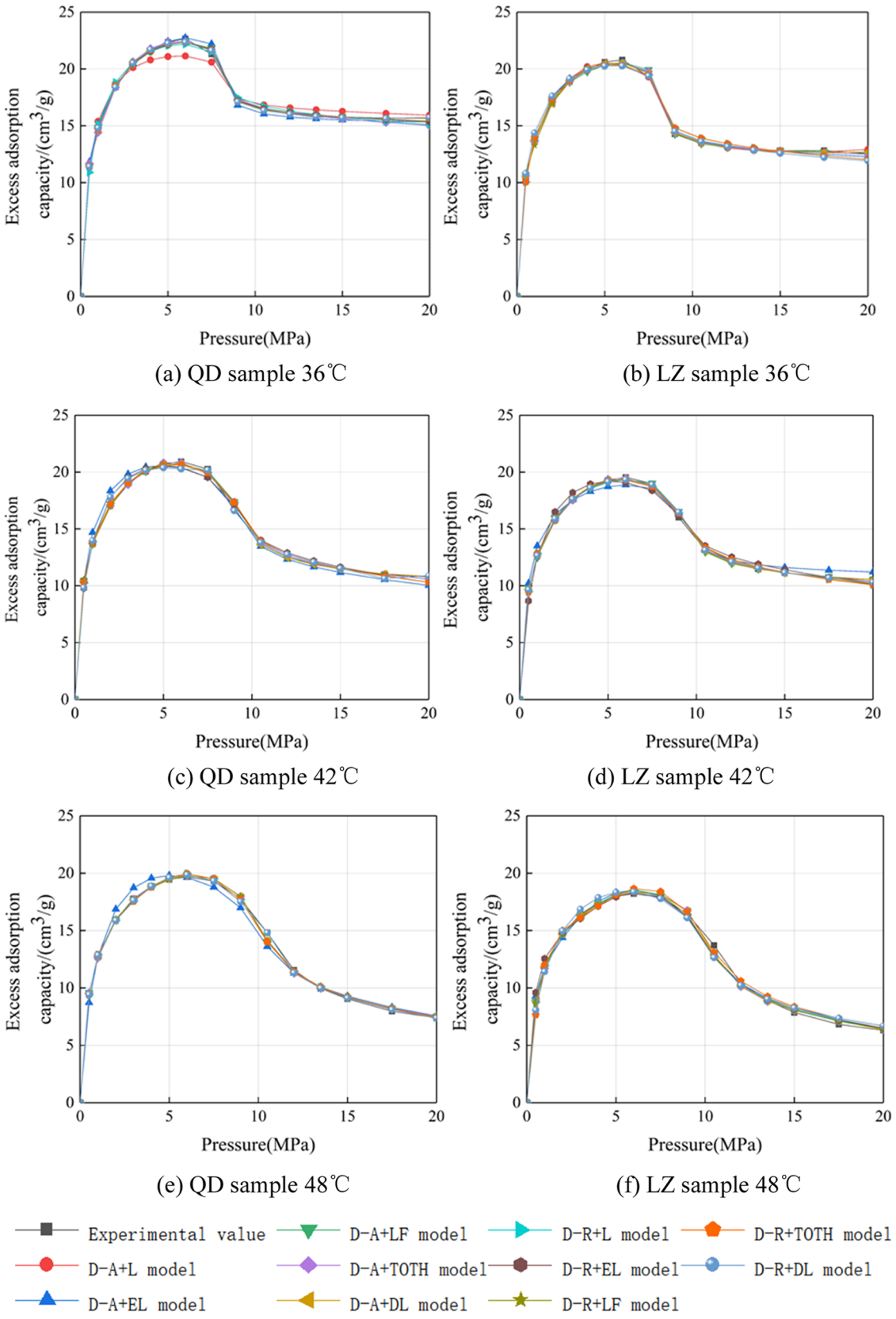

Figure 10. Excess adsorption curves for micropore filling superimposed on a single molecule adsorption model.

the solid surface determines the surface adsorption potential.[44] The micropores exhibit much larger curvatures compared with the transition pores and mesopores, resulting in a higher adsorption potential for the micropore surface, which enables preferential adsorption of CO_2 molecules. However, the transition pores also possess a certain adsorption potential and exert a certain adsorption effect on the CO_2 molecules.

https://doi.org/10.1021/acsomega.3c06599
ACS Omega 2023, 8, 44195−44211

Table 9. Mixed Adsorption Model Fitting Parameters, RMSE, and Coefficient of Determination (R^2)

		QD sample			LZ sample		
mixed model	parameters	36 °C	42 °C	48 °C	36 °C	42 °C	48 °C
intercept method	$V(cm^3/g)$	24.031	23.264	23.214	22.445	21.697	21.719
	$\rho_a(g/cm^3)$	2.3361	1.5178	1.1930	1.8710	1.5810	1.1483
DA-L	V	27.997	27.561	24.970	24.044	25.656	23.705
	ρ_a	1.865	1.370	1.214	1.710	1.392	1.010
	R^2	0.999	0.998	0.997	0.998	0.999	0.997
	RMSE	0.480	0.527	0.527	0.516	0.385	0.712
DA -EL	V	28.303	27.009	27.689	26.002	23.561	27.496
	ρ_a	1.669	1.488	1.270	1.617	1.405	1.209
	R^2	0.996	0.990	0.990	0.998	0.993	0.996
	RMSE	0.887	1.562	1.625	0.669	1.304	0.930
DA-LF	V	26.321	28.480	26.495	27.614	26.276	22.954
	ρ_a	1.644	1.318	1.093	1.184	1.077	1.209
	R^2	0.999	0.999	0.998	0.998	0.998	0.997
	RMSE	0.876	0.607	1.147	2.362	1.725	1.198
DA-TOTH	V	25.280	23.531	24.803	24.053	22.121	23.248
	ρ_a	1.935	1.367	1.072	1.623	1.391	1.080
	R^2	0.998	0.999	0.9982	0.998	0.999	0.997
	RMSE	0.367	0.450	0.602	0.339	0.328	0.427
DA-DL	V	27.894	27.218	25.136	28.305	26.140	24.986
	ρ_a	1.970	1.381	1.088	1.609	1.413	1.032
	R^2	0.999	0.9990	0.998	0.999	0.999	0.997
	RMSE	0.341	0.437	0.601	0.338	0.309	0.692
DR-L	V	26.351	24.805	24.971	24.600	23.102	23.363
	ρ_a	2.204	1.523	1.214	1.801	1.597	1.173
	R^2	0.996	0.997	0.997	0.995	0.998	0.996
	RMSE	0.888	0.665	0.695	0.941	0.584	0.820
DR-EL	V	27.712	26.402	24.974	24.629	24.009	23.991
	ρ_a	1.968	1.669	0.9978	1.801	1.768	1.202
	R^2	0.998	0.994	0.995	0.995	0.991	0.994
	RMSE	0.531	1.130	0.695	0.941	1.239	1.135
DR-LF	V	24.962	24.297	23.861	23.389	22.867	22.821
	ρ_a	2.245	1.498	1.196	1.814	1.546	1.135
	R^2	0.997	0.998	0.997	0.996	0.998	0.9968
	RMSE	0.618	0.544	0.659	0.605	0.452	0.793
DR-TOTH	V	26.350	24.804	24.770	24.600	23.102	22.065
	ρ_a	2.204	1.523	1.214	1.801	1.596	1.265
	R^2	0.996	0.997	0.997	0.995	0.998	0.992
	RMSE	0.888	0.665	0.695	0.941	0.585	1.301
DR-DL	V	26.304	25.396	25.038	26.009	24.896	24.251
	ρ_a	2.213	1.461	1.235	1.701	1.461	1.141
	R^2	0.996	0.998	0.992	0.994	0.999	0.992
	RMSE	0.888	0.534	1.429	1.040	0.396	1.246

4.3. Optimization of the Adsorption Model. Further, the mixed models of microporous filling theory and monocular theory were compared and analyzed, and 10 kinds of mixed models were used to fit the CO_2 excess adsorption curves of two coal samples at 36, 42, and 48 °C. As shown in Figure 10, all models have good fitting effects in the entire pressure segment (0−20 MPa). The determination coefficients, root-mean-square errors, and fitting parameters of the 10 mixed models are shown in Table 9. It can be seen from Table 9 that the R^2 value of each model is higher than 0.99. The comparison with the R^2 of Table 6 shows that the fitting effect of the mixed model on the excess adsorption curve is better than that of the single adsorption theoretical model. Through RMSE, it can be found that the mixed models of DA-L, DA-TOTH, DA-DL, DR-L, and DR- LF have better fitting effects. Because the fitting results of the model are based on the best coefficient of determination R^2, the accuracy of the model parameters may be ignored. Therefore, it is necessary to analyze further the theoretical adsorption capacity and adsorption phase density of the model parameters to optimize the optimal model. According to the above analysis and literature research results, both the theoretical adsorption capacity of model parameters and the adsorption phase density decrease with an increase in temperature. It can be seen from Table 9 that the theoretical adsorption capacity and adsorption phase density of the mixed model parameters of DA-DL, DR-EL, DR-LF, DR -TOTH, and DR-DL have good physical significance. It is further shown that the DR model is superior to the DA model in the micropore filling theory. However, the errors in the model parameters need to be analyzed to obtain the most suitable model to fit the coal adsorption of $ScCO_2$.

In this paper, the fitted adsorption phase density ρ_a in Table 8 was compared with the adsorption phase density obtained by the

https://doi.org/10.1021/acsomega.3c06599
ACS Omega 2023, 8, 44195−44211

Table 10. Standard Errors (S) of Adsorption Phase Density between Those Simulated by Mixed Adsorption Models and the Intercept Method at Different Temperatures

	36 °C		42 °C		48 °C		
adsorption model	LZ	QD	LZ	QD	LZ	QD	average
DA-L	0.161	0.471	0.189	0.148	0.138	0.021	0.188
DA-EL	0.254	0.667	0.176	0.03	0.061	0.077	0.21
DA-LF	0.687	0.692	0.504	0.2	0.061	0.1	0.374
DA-TOTH	0.248	0.401	0.19	0.151	0.068	0.121	0.196
DA-DL	0.262	0.366	0.168	0.137	0.116	0.105	0.192
DR-L	0.007	0.132	0.187	0.005	0.054	0.021	0.045
DR-EL	0.007	0.368	0.187	0.151	0.054	0.195	0.171
DR-LF	0.057	0.091	0.035	0.019	0.013	0.03	0.036
DR-TOTH	0.07	0.132	0.015	0.005	0.117	0.021	0.06
DR-DL	0.17	0.123	0.12	0.057	0.007	0.042	0.087

Table 11. Relative Error (∂) between Each Adsorption Theoretical Model and the Intercept Method Theoretical Adsorption Capacity

	36 °C		42 °C		48 °C		
adsorption model	LZ (%)	QD (%)	LZ (%)	QD (%)	LZ (%)	QD (%)	average (%)
DA-L	16.50	18.47	7.56	7.12	18.25	9.14	12.84
DA-EL	17.78	16.10	19.28	15.85	8.59	26.60	17.36
DA-LF	9.53	22.42	14.13	23.03	21.10	5.69	15.98
DA-TOTH	5.20	1.15	6.85	7.16	1.95	7.04	4.89
DA-DL	16.08	17.00	8.28	26.11	20.48	15.04	17.16
DR-L	9.65	6.62	7.57	9.60	6.48	7.57	7.92
DR-EL	15.32	13.49	7.58	9.73	10.66	10.46	11.21
DR-LF	3.87	4.44	2.79	4.21	5.39	5.07	4.30
DR-TOTH	9.65	6.62	7.56	9.60	6.48	1.59	6.92
DR-DL	9.46	9.16	7.86	15.88	14.74	11.66	11.46
L	11.46	11.31	12.22	11.47	11.27	12.06	11.63
LF	4.11	15.14	4.01	15.37	12.16	19.95	11.79
EL	11.64	18.48	10.51	18.27	17.13	20.51	16.09
TOTH	11.47	23.45	11.16	7.76	4.61	12.22	11.78
D−R	9.80	0.19	10.46	0.22	5.69	1.24	4.60

intercept method as the standard error in eq 10 to compare the accuracy of the models. The standard error S values of the parameter adsorption phase density in the calculated adsorption models are shown in Table 10. The smaller the standard error S, the more accurate the fitted adsorption phase density of the model and the more accurately it can describe the adsorption behavior of CO_2 in coal. From the mean values of standard errors of adsorption phase densities fitted by the 10 mixed adsorption models at different temperatures of two coal samples, the exact order can be obtained as follows: DR-LF > DR-L > DR-TOTH > DR-DL > DR-EL > DA-L > DA-DL > DA-TOTH > DA-EL > DA-LF. The standard error S values of the DR-LF model are much smaller than those of the other mixed adsorption models and the seven single adsorption models in Table 8, indicating that this model can more accurately reflect the adsorption process of $ScCO_2$ in the nanopores of coal.

To further analyze the difference between the model fitting parameter theoretical adsorption capacity and the intercept method, the relative error (∂) is introduced to evaluate the calculated results.

$$\partial = |V_a\rho_a - V|/V_a\rho_a \times 100\% \quad (11)$$

The 5 types of modified adsorption models, L, LF, EL, TOTH, and D−R, fitted more accurately in the previous paper, were selected to compare and evaluate the relative error (∂) of theoretical adsorption capacity with 10 types of mixed adsorption models. As seen from Table 11, the average relative error of theoretical adsorption capacity predicted by the adsorption model D−R was lower in different coal samples but fluctuated more. The relative errors predicted by the newly developed DR-LF model in this paper were overwhelmingly below 5% at 36, 42, and 48 °C, with a mean value of 4.30%, much lower than other models. The relative errors indicate that the model has a high prediction accuracy. The error analysis of the theoretical adsorption of some models has also been carried out in previous studies,[45] and the error of the theoretical adsorption is greater compared to the theoretical adsorption of the DR-LF model preferred in this paper. Tables 10 and 11 show that the DR-LF adsorption model of coal CO_2 high-pressure adsorption, consisting of the adsorption equation mixed with different adsorption theories, can accurately fit the coal CO_2 high-pressure adsorption curve. The modified absolute adsorption capacity is reasonable and accurate. Compared with the existing models, this model is more consistent with the adsorption mechanism of CO_2 on coal and has a better physical basis.

Combined with the above analyses, the DR-LF mixed model is the best model to predict the adsorption capacity of coal for $ScCO_2$. The parameter λ of the DR-LF model was used to analyze further the contribution of different adsorption mechanisms to the excess adsorption of $ScCO_2$ in coal. The theoretical adsorption capacity proportion of the LZ and QD

https://doi.org/10.1021/acsomega.3c06599
ACS Omega 2023, 8, 44195−44211

coal samples under different adsorption theories at different temperatures is shown in Table 12.

Table 12. Microporous Filling Theory and Monomolecular Layer Adsorption Theory Adsorption Proportion (λ)

	LZ			QD		
adsorption proportion	36 °C	42 °C	48 °C	36 °C	42 °C	48 °C
λ (%)	55.7	67.6	81.7	55.8	69.5	80.0
$1-\lambda$ (%)	44.3	32.4	18.3	44.2	30.5	20.0

As can be seen from Table 12, the CO_2 micropore-filled adsorption in the LZ and QD samples was consistently higher than the monomolecular layer adsorption in the transition pores and mesopores, where the micropore-filled adsorption was greater than 50% in all cases. It was concluded in the literature[46] through a combination of theory and experiment that the specific surface area (SSA) of micropores in coal accounted for 90.39% of the total SSA. The adsorption in the form of microporous filling accounted for 74% of the total adsorption. In this article, the microporous SSA in LZ and QD samples were 73.19 and 71.99%, respectively. The adsorption in the form of microporous filling capacity was 55.7−81.7% of the total adsorption in the LZ samples and 55.8−80% of the total adsorption in the form of microporous filling in the QD samples, which showed a good correlation with the previous studies. It can be found that the adsorption proportion of the microporous filled form increases with increasing temperature, and the adsorption of CO_2 on the coal surface is a typical exothermic process, and increasing temperature is not conducive to the adsorption of CO_2. As the temperature increases, the kinetic energy of the CO_2 molecules increases. According to Table 3, the proportion from the micropore and the transition pore is beyond 50%, which provides the adsorption space for microporous filling adsorption of CO_2. Meanwhile, in some adsorption sites with weaker adsorption force, the smaller pore size of the micropores results in greater curvature. The superposition of the adsorption potential occurs, leading to stronger micropores for the CO_2 adsorption capacity than mesopores and macropores. It is more difficult for the CO_2 molecules in the micropores to change into free phase CO_2 during the warming process. Therefore, the higher the temperature, the higher the contribution of the microporous filling adsorption theory to the adsorption capacity and the lower the contribution of the monomolecular layer adsorption capacity of the transition pores and mesopores to the total adsorption capacity.

5. CONCLUSIONS

This paper investigated the $ScCO_2$ adsorption characteristics of a low-permeability coal seam in the Huainan−Huaibei coalfield in China. Based on 9 modified adsorption models, 14 mixed adsorption models were constructed to fit the experimentally obtained high-pressure adsorption isotherms at 36, 42, and 48 °C. The errors of adsorption phase density and theoretical adsorption amount based on the fitted parameters were compared and analyzed to select the best adsorption model. The conclusions can be summarized as follows:

(1) The L, LF, EL, and TOTH models of the monomolecular layer adsorption theory are suitable for fitting the CO_2 excess adsorption capacity in coal at the low-pressure stage (pressures lower than 7.5 MPa), and the DR model of the micropore filling adsorption theory is suitable for fitting the CO_2 excess adsorption capacity in coal at the high-pressure stage (pressures higher than 7.5 MPa). The theoretical model of multimolecular layer adsorption is unsuitable for fitting the excess adsorption capacity of $ScCO_2$ in coal.

(2) Among the mixed models developed for different adsorption theories, the multimolecular layer adsorption theory did not contribute to the adsorption capacity, which initially reveals that the mixed model of multimolecular layer and microporous filling theories is not suitable for fitting the excess adsorption of CO_2 by coal.

(3) The analysis of the standard error of the adsorption phase density and the relative error of the theoretical adsorption capacity obtained with the intercept method showed that the mixed monomolecular layer and micropore filling theory adsorption model of DR-LF could predict the coal adsorption capacity of $ScCO_2$ more accurately than the 9 modified and other mixed models.

(4) The results of the DR-LF mixed model based on the theory of monomolecular layer adsorption and micropore-filled adsorption showed that the proportion of CO_2 adsorption in the form of micropore-filled adsorption in coal increased gradually with the increase of temperature, and the contribution of micropore-filled adsorption to the total adsorption was always more than 50%.

AUTHOR INFORMATION

Corresponding Authors

Huihu Liu − *School of Earth and Environment, Anhui University of Science & Technology, Huainan 232001, China; Institute of Energy, Hefei Comprehensive National Science Center, Hefei 230031, China;* orcid.org/0000-0002-6703-0357; Email: xixiinformation@163.com

Sheng Xue − *Institute of Energy, Hefei Comprehensive National Science Center, Hefei 230031, China; School of Safety Science and Engineering, Anhui University of Science and Technology, Huainan 232001, China*; Email: sheng.xue@aust.edu.cn

Authors

Zhengpu Fan − *School of Earth and Environment, Anhui University of Science & Technology, Huainan 232001, China;* orcid.org/0009-0004-0079-1858

Junlin Liu − *School of Earth and Environment, Anhui University of Science & Technology, Huainan 232001, China*

Kun Zhang − *School of Earth and Environment, Anhui University of Science & Technology, Huainan 232001, China*

Hongjie Xu − *School of Earth and Environment, Anhui University of Science & Technology, Huainan 232001, China*

Huihuang Fang − *School of Earth and Environment, Anhui University of Science & Technology, Huainan 232001, China*

Complete contact information is available at: https://pubs.acs.org/10.1021/acsomega.3c06599

Notes

The authors declare no competing financial interest.

ACKNOWLEDGMENTS

This work was financially supported by the National Natural Science Foundation of China (Grant No. 42277483), the Anhui Provincial Natural Science Foundation (2008085MD121 and 2108085MD134), the Institute of

https://doi.org/10.1021/acsomega.3c06599
ACS Omega 2023, 8, 44195−44211

Energy, Hefei Comprehensive National Science Center (Grant No. 21KZS218), the Key Scientific Research Foundation of the Education Department of Province Anhui (Grant No. KJ2020A0317), and the Anhui Provincial Key Research and Development Project (Grant No. 2023z04020001).

REFERENCES

(1) Cheng, X.; Cheng, Y.; Hu, B.; et al. Quantitative analysis of the difference in CH_4 and CO_2 adsorption capacity in coal based on adsorption model. *J. Nat. Gas Sci. Eng.* **2022**, *102*, No. 104541.
(2) Aminu, M. D.; Nabavi, S. A.; Rochelle, C. A.; Manovic, V. A review of developments in carbon dioxide storage. *Appl. Energy* **2017**, *208*, 1389−1419.
(3) Benson, S. M.; Cole, D. R. CO_2 sequestration in deep sedimentary formations. *Elements* **2008**, *4* (5), 325−331.
(4) Diao, R.; Zhang, H.; Zhao, D.; Li, S. CH_4 and CO_2 adsorption-induced deformation of carbon slit pores with implications for CO_2 sequestration and enhanced CH_4 recovery. *J. CO_2 Util.* **2019**, *32*, 66−79.
(5) Lie, H.; Zhang, J.; Ma, X.; Bian, R. A preliminary investigation of negative adsorption phenomenon of shale isothermal adsorption gas content. *Earth Sci. Front.* **2013**, *20* (06), 282−288.
(6) Ju, Y.; Jiang, B.; Hou, Q.; Tan, Y.; Wang, G.; Xiao, W. Behavior and mechanism of the adsorption/desorption of tectonically deformed coals. *Chin. Sci. Bull.* **2009**, *54* (1), 88−94.
(7) Shen, R.; Gou, H.; Hu, Z.; Xiong, W.; Zuo, L. High pressure adsorption characteristics of shale gas and its impact on storage and recovery patterns. *Earth Sci. Front.* **2018**, *25* (02), 204−209.
(8) Liu, C.; Zhang, Y.; Jia, T.; Zhong, F. New interpretation of adsorption test mechanism and adsorption law for gas source rock. *J. China Coal Soc.* **2019**, *44* (11), 3441−3452.
(9) Yu, H.; Fan, W.; Sun, M.; Ye, J. Isothermal adsorption properties of coal on CH_4/CO_2 binary gas and its prediction. *J. China Coal Soc.* **2005**, *30* (5), 618−622.
(10) Liu, H.; Sang, S.; Liu, S.; Wu, H.; Lan, T.; Xu, H.; Ren, B. Supercritical-CO_2 adsorption quantification and modeling for a deep coalbed methane reservoir in the southern Qinshui Basin, China. *ACS Omega* **2019**, *4* (7), 11685−11700.
(11) Ozdemir, E. Dynamic nature of supercritical CO_2 adsorption on coals. *Adsorption* **2017**, *23* (1), 25−36.
(12) Pini, R.; Ottiger, S.; Burlini, L.; Storti, G.; Mazzotti, M. Sorption of carbon dioxide, methane and nitrogen in dry coals at high pressure and moderate temperature. *Int. J. Greenhouse Gas Control* **2010**, *4* (1), 90−101.
(13) Weniger, P.; Francu, J.; Hemza, P.; Krooss, B. M. Investigations on the methane and carbon dioxide sorption capacity of coals from the SW Upper Silesian Coal Basin, Czech Republic. *Int. J. Coal Geol.* **2012**, *93*, 23−39.
(14) Bae, J. S.; Bhatia, S. K. High-pressure adsorption of methane and carbon dioxide on coal. *Energy Fuels* **2006**, *20* (6), 2599−2607.
(15) Tang, X.; Ripepi, N.; Stadie, N. P.; Yu, L.; Hall, M. R. A dual-site Langmuir equation for accurate estimation of high pressure deep shale gas resources. *Fuel* **2016**, *185*, 10−17.
(16) Wu, D.; Liu, X.; Sun, K.; Xiao, X.; Xin, L. Experiments on supercritical CO_2 adsorption in briquettes. *Energy Sources, Part A* **2019**, *41* (8), 1005−1011.
(17) Xue, J.; Fu, X.; Fan, C.; Song, D. Adsorption and adsorption model of H_2S in different coal ranks. *Coal Geol. Explor.* **2016**, *44* (06), 75−78.
(18) Jiang, Y.; Song, X.; Liu, H.; Zheng, Q.; Liang, Y.; Cui, Y.; et al. Adsorption model and law of methane under the effect of high-power acoustic wave. *J. China Coal Soc.* **2014**, *39* (S1), 152−157.
(19) Day, S.; Duffy, G.; Sakurovs, R.; Weir, S. Effect of coal properties on CO_2 sorption capacity under supercritical conditions. *Int. J. Greenhouse Gas Control* **2008**, *2* (3), 342−352.
(20) He, J.; Shi, Y.; Ahn, S.; Kang, J. W.; Lee, C. H. Adsorption and desorption of CO_2 on Korean coal under subcritical to supercritical conditions. *J. Phys. Chem. B* **2010**, *114* (14), 4854−4861.
(21) Feng, Z.-c.; Cai, T.; Zhou, D.; Zhao, D.; Zhao, Y.; Wang, C. Temperature and deformation changes in anthracite coal after methane adsorption. *Fuel* **2017**, *192*, 27−34.
(22) Moore, T. A. Coalbed methane: a review. *Int. J. Coal Geol.* **2012**, *101*, 36−81.
(23) Zhou, S.; Wang, H.; Xue, H.; Guo, W.; Li, X. Shale gas supercritical adsorption mechanism and model. *Chin. Sci. Bull.* **2017**, *62* (35), 4189−4200.
(24) Liu, X.; Zhang, L.; Li, S.; Zhang, J.; Zhao, Y.; Zhang, R.; et al. Supercritical methane isothermal sorption model considering multiple sorption mechanisms in shale. *Acta Petrolei Sin.* **2022**, *43* (10), 1487−1499.
(25) Hou, X.; Wang, M.; Liu, Yu.; Liu, J.; Song, Y. Shale gas supercritical state adsorption model and its geological significance. *J. China Univ. Min. Technol.* **2016**, *45* (01), 111−118.
(26) Li, Y.; Zuo, J.; Yao, M.; Liu, D.; Chen, G. Optimization of supercritical isothermal adsorption model and reservoir calculation for shale gas. *J. China Univ. Min. Technol.* **2019**, *48* (02), 322−332.
(27) Currie, L. A. Nomenclature in evaluation of analytical methods including detection and quantification capabilities: (IUPAC Recommendations 1995). *Anal. Chim. Acta* **1999**, *391* (2), 105−126.
(28) Langmuir, I. The constitution and fundamental properties of solids and liquids. II. Liquids. *J. Am. Chem. Soc.* **1917**, *39* (9), 1848−1906.
(29) Langmuir, I. The adsorption of gases on plane surfaces of glass, mica and platinum. *J. Am. Chem. Soc.* **1918**, *40* (9), 1361−1403.
(30) Rushton, G. T.; Karns, C. L.; Shimizu, K. D. A critical examination of the use of the Freundlich isotherm in characterizing molecularly imprinted polymers (MIPs). *Anal. Chim. Acta* **2005**, *528* (1), 107−113.
(31) Tóth, J. Modifications in classic relationships corresponding to gas/solid physical adsorption. *J. Colloid Interface Sci.* **1997**, *191* (2), 449−455.
(32) Xie, L.; Li, Q.; Demir, M.; Yu, Q.; Hu, X.; Jiang, Z.; Wang, L. Lotus seed pot-derived nitrogen enriched porous carbon for CO_2 capture application. *Colloids Surf., A* **2022**, *655*, No. 130226.
(33) Dubinin, M.; Astakhov, V. Development of the concepts of volume filling of micropores in the adsorption of gases and vapors by microporous adsorbents: Communication 1. Carbon adsorbents. *Bull. Acad. Sci. USSR, Div. Chem. Sci.* **1971**, *20*, 3−7.
(34) Dubinin, M. M. The equation of the characteristic curve of activated charcoal. *Dokl. Akad. Nauk SSSR* **1947**, *55*, 327−329.
(35) Wu, D.; Miao, F.; Liu, X.; Xiao, X.; Zhai, W. Prediction of high-pressure adsorption of CH_4 and CO_2 in shale. *Int. J. Greenhouse Gas Control* **2021**, *110*, No. 103440.
(36) Kim, H. J.; Shi, Y.; He, J.; Lee, H. H.; Lee, C. H. Adsorption characteristics of CO_2 and CH_4 on dry and wet coal from subcritical to supercritical conditions. *Chem. Eng. J.* **2011**, *171* (1), 45−53.
(37) Liu, H.; Liu, J.; Xue, S.; Zhang, K.; Xu, H.; Fang, H.; Jia, J. Insight into difference in high-pressure adsorption-desorption of CO_2 and CH_4 from low permeability coal seam of Huainan-Huaibei coalfield, China. *J. Environ. Chem. Eng.* **2022**, *10* (6), No. 108846.
(38) Cao, L.; Tianrang, J.; Fuping, Z.; Guoying, W. Establishing a New Piecewise Method for Understanding and Rectifying Mass Balance Miscalculation of Gas Adsorption on Coal and Shale. *Energy Fuels* **2021**, *35* (5), 4283−4295.
(39) Yao, Y.; Liu, D.; Huang, W.; Tang, S. Research on the pore fractures system properties of coalbed methane reservoirs and recovery in Huainan and Huaibei coal fields. *J. China Coal Soc.* **2006**, *02*, 163−168.
(40) Li, J.; Yao, Y.; Cai, Y.; Qiu, Y. Discussion on coal physical properties and formation with different metamorphic degree in North China. *Coal Sci. Technol.* **2012**, *04*, 111−115.
(41) Lu, Y.; Ao, X.; Tang, J.; et al. Swelling of shale in supercritical carbon dioxide. *J. Nat. Gas Sci. Eng.* **2016**, *30*, 268−275.
(42) Hu, B.; Cheng, Y.; Pan, Z. Classification methods of pore structures in coal: A review and new insight. *Gas Sci. Eng.* **2023**, *110*, No. 204876.

https://doi.org/10.1021/acsomega.3c06599
ACS Omega 2023, 8, 44195−44211

(43) Song, Y.; Xing, W.; Zhang, Y.; et al. Adsorption isotherms and kinetics of carbon dioxide on Chinese dry coal over a wide pressure range. *Adsorption* **2015**, *21*, 53−65.
(44) Meng, Z.; Liu, S.; Li, G. Adsorption capacity, adsorption potential and surface free energy of different structure high rank coals. *J. Pet. Sci. Eng.* **2016**, *146*, 856−865.
(45) Atanu, C.; Santanu, B.; Pratik, D. Methane/CO_2 binary gas interaction on some moist, high−volatile bituminous Indian coals: 2. Pure-/mixed-gas adsorption modelling. *J. Pet. Sci. Eng.* **2022**, *208*, No. 109673.
(46) Hu, B.; Cheng, Y.; He, X.; Wang, Z.; Jiang, Z.; Wang, C.; Li, W.; Wang, L. New insights into the CH_4 adsorption capacity of coal based on microscopic pore properties. *Fuel* **2020**, *262*, No. 116675.

https://doi.org/10.1021/acsomega.3c06599
ACS Omega 2023, 8, 44195−44211